sustainability

MDPI

Article

Exploring the Evolution of Permafrost on the Tibetan Plateau (1979–2100) Using the Temperature at the Top of Permafrost (TTOP) Model: Implications for Sustainable Development

Jiahao Wei and Shangmin Zhao *

College of Geological and Surveying Engineering, Taiyuan University of Technology, Taiyuan 030024, China; 2023510723@link.tyut.edu.cn

* Correspondence: zhaoshangmin@tyut.edu.cn; Tel.: +86-13623621189

Abstract

The permafrost in the Tibetan Plateau is extremely sensitive to climate warming, which poses challenges to regional sustainability. Predicting the evolution of permafrost on the Tibetan Plateau in the future could provide a reference for future engineering, construction, and resource management on the Tibetan Plateau. In this study, the Random Forest regression model and the temperature at the top of permafrost (TTOP) model are combined. The Random Forest regression model is used to simulate the long-term series of land surface temperatures. The multiple climate model data sets in the Coupled Model Intercomparison Project Phase 6 (CMIP6) and TTOP model are used to simulate the historical (1979–2018) and predict the future (2019–2100) distribution of permafrost on the Tibetan Plateau. The results show that since 1979, due to climate warming, more than 20% of the permafrost in the Tibetan Plateau has disappeared. The permafrost will degrade at different rates under each of four Shared Socioeconomic Pathways (SSPs), namely SSP1–2.6, SSP2–4.5, SSP3–7.0, and SSP5–8.5. The degradation rate under SSP1–2.6 is the slowest, indicating that about 20.1% of the permafrost will disappear by 2100. The degradation rate under the SSP5–8.5 is the fastest, predicting that about 82.4% of the permafrost will disappear by 2100. Under SSP2–4.5 and SSP3–7.0, 37.57% and 69.1% of the permafrost will disappear by 2100, respectively. The above results can provide a reference for sustainable engineering construction, infrastructure planning, and climate adaptation strategies on the Tibetan Plateau.

Keywords: permafrost; Tibetan Plateau; sustainable development; climate warming; random forest; quantile mapping; CMIP6

Check for updates

Academic Editor: Antonio Miguel Martínez-Graña

Received: 26 April 2026
Revised: 26 May 2026
Accepted: 29 May 2026
Published: 2 June 2026

Copyright: © 2026 by the authors. Licensee MDPI, Basel, Switzerland. This article is an open access article distributed under the terms and conditions of the Creative Commons Attribution (CC BY) license.

1. Introduction

Permafrost, defined as subsurface earth materials remaining below 0 °C for two consecutive years, is mainly distributed in the Arctic region and the Tibetan Plateau (TP) region, where permafrost regions occupy 22% of the exposed land surface area [1,2]. The TP is the most widely distributed region of mid-latitude permafrost in the world [3]. Due to its unique geographical characteristics, permafrost on the TP is more sensitive to air temperature changes compared to high-latitude permafrost regions [4,5]. Currently, both air and land surface temperatures on the TP are rising at a rate exceeding the global average for land areas [6], leading to significant permafrost degradation. This degradation can release organic carbon, increase greenhouse gas emissions, and create a positive feedback loop that further accelerates warming and thawing [7]. Permafrost degradation also induces ground deformation and landslides, posing geohazards [8], damaging infrastructure

such as railways and highways [9], reducing groundwater storage, and exacerbating desertification [10]. Consequently, obtaining high-resolution, high-precision spatiotemporal information on permafrost evolution is a pressing need for engineering planning and climate risk assessment in the cold regions of the TP.

Key indicators for permafrost research include active layer thickness, maximum freezing depth, and permafrost distribution, with the latter being one of the most effective measures of its response to climate warming. Early researchers mapped permafrost distribution manually using satellite imagery and field surveys [11]. With advancing methodologies, Zou et al. [12] employed the temperature at the top of permafrost (TTOP) model to generate a high-resolution permafrost map of the TP, estimating a coverage of approximately 1.06×10^6 km^2, providing a new methodology for permafrost studies. Aalto et al. [13] modeled mean annual ground temperature ($MAGT$) and active layer thickness using various techniques, successfully simulating Northern Hemisphere permafrost distribution at a 1 km resolution. Marcer et al. [14] used a hybrid statistical-numerical approach to model rock temperatures in West Greenland, determining permafrost presence based on rock surface temperature and validating the model with borehole data. Other methods have also shown success, such as the surface frost number model [15], machine learning techniques like Random Forest and Support Vector Machines [16], and the Stefan equation for predicting freeze-thaw depth [17,18]. In recent years, the dichotomy between purely data-driven machine learning methods and purely physics-based numerical models has been progressively bridged by physics-guided hybrid algorithms that integrate observational data with physical constraints. Such approaches have demonstrated improved predictive accuracy while maintaining physical consistency in various engineering domains [19,20]. Among these, the TTOP model, with its few parameters and high computational efficiency, is particularly suitable for large-scale permafrost simulation [21], especially in data-sparse, high-latitude, and high-altitude regions (e.g., Smith and Riseborough [22], 2002 in Canada; Li et al. [23], 2022 in Northeast China). Therefore, the TTOP model combining machine learning and data-driven models is selected as the preferred method basis of this study.

The TTOP model only requires surface temperature (or air temperature) and soil properties as input parameters, so some researchers have combined the temperature prediction data in CMIP6 with the TTOP model to predict the spatial and temporal evolution of permafrost in the future. Li et al. [24] used CMIP6 data, the TTOP model, and a modified Stefan equation to study the spatiotemporal changes in $MAGT$, permafrost distribution, and active layer thickness on the TP for past, present, and future periods. They concluded that permafrost would continuously degrade under all future scenarios, with approximately 18.80%, 40.81%, 56.96%, and 63.28% lost by the end of the 21st century, respectively. Zhao et al. [25] conducted a similar study using CMIP6 and TTOP, affirming continuous degradation but projecting more severe losses, with permafrost area reducing to 75%, 49%, 29%, and 17% of the current area (2010–2018) under SSP1–2.6, SSP2–4.5, SSP3–7.0, and SSP5–8.5, respectively. However, these similar studies typically employ the Delta method for downscaling coarse-resolution future climate data. This method calculates the bias between historical high-resolution and low-resolution data and applies this bias to future low-resolution data. It assumes the probability distribution of future climate is identical to that of the historical period, failing to capture future spatial heterogeneity changes and underestimating future extreme temperatures. Therefore, this study adopts an alternative downscaling method: Quantile Mapping (QM). QM can more effectively correct systematic biases in climate models, and (with sufficient training samples) provide superior calibration for extreme climate events, which the linear correction of the Delta method cannot achieve [26,27]. In addition, future climate predictions lack LST data. When applying the TTOP model to future scenarios, it is necessary to calculate the ratio of the

surface freeze-thaw index to the atmospheric freeze-thaw index in the historical period, that is, the n-factor, to correct the difference between the air and surface freeze-thaw index [24,25]. Zou et al. [12] bypassed this by directly using MODIS_LST data to calculate surface freezing/thawing indices, obtaining a high-precision permafrost map. This study uses a Random Forest regression model to learn the mapping relationship between air temperature and LST from historical data and then apply it to future predictions. This method is more flexible than extrapolation by ratio, which increases the accuracy of the TTOP model for future prediction.

Therefore, this study integrates QM downscaling and a machine learning-driven parameter optimization scheme to enhance the performance of the TTOP model and investigate the spatiotemporal evolution of permafrost on the TP from 1979 to 2100 under different climate change scenarios, aiming to provide a more reliable, high-resolution future permafrost projection to support sustainable engineering, construction, and resource management on the TP.

2. Materials and Methods

The study area is the Tibetan Plateau (TP), located between 26°00′–39°47′ N and 73°19′–104°47′ E (Figure 1). It is bounded by the Himalayas to the south, the Kunlun and Qilian Mountains to the north, the Pamir Plateau and Karakoram Mountains to the west, the Qinling Mountains and Loess Plateau to the east and northeast. As the largest and highest plateau in China, it is often referred to as the "Roof of the World."

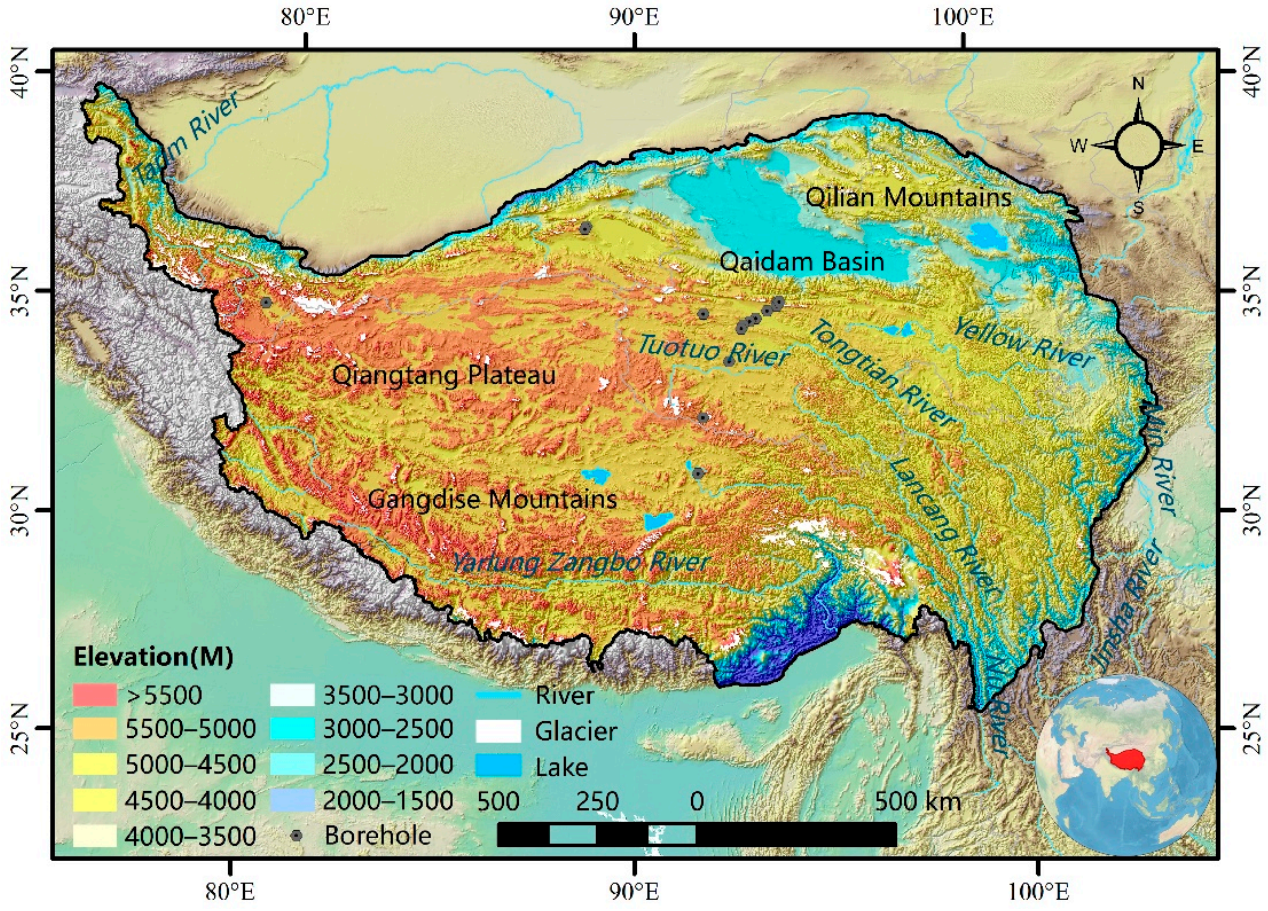


Figure 1. Overview of the Tibetan Plateau.

The TP is the headwater region for numerous major rivers, including the Yellow River, Yangtze River, Yarlung Zangbo River, and Ganges River. These rivers meander across the

plateau, forming extensive watersheds. In addition to rivers, the TP hosts numerous lakes, such as Qinghai Lake and Pangong Tso. The region possesses abundant water resources, and permafrost degradation impacts its water cycle and supply [28], being a primary contributor to the declining water levels in the Yangtze and Yellow Rivers [29].

The TP features many mountain ranges, including the Kunlun, Himalayas, Gangdise, and Qilian Mountains, with average elevations exceeding 5000 m. Their peaks are perpetually snow-capped and glaciated. Year-round temperatures in these regions are below 0 °C, and most areas are underlain by permafrost.

This study focuses on simulating historical permafrost distribution and projecting its future distribution on the TP using the TTOP model. For the historical period (1979–2018), simulations were conducted at ten-year intervals. For the future period (2019–2100), projections were made at twenty-year intervals under different SSP scenarios to investigate their varying degradation trends.

2.1. Temperature at the Top of Permafrost Model

The temperature at the top of permafrost (TTOP) is a critical indicator of the permafrost's thermal state. The model was initially proposed by Smith and Riseborough [30] and has since been widely applied in permafrost regions. It integrates the influences of air temperature, surface, and soil factors on the ground thermal regime to simulate the spatial $MAGT$ [31], constituting a physics-based model with multiple parameters. The most used formula versions are as follows [24]:

$$MAGT = \frac{\left(k_t / k_f \times n_t \times I_t\right) - \left(n_f \times I_f\right)}{P} \quad (1)$$

where P is the annual period (days), typically 365; k_t and k_f are the thermal conductivities of the active layer in the thawed and frozen states, respectively; n_t and n_f are correction factors (n-factors) for converting the air freezing/thawing indices to the surface indices, n_t is the ratio of the air thawing index to the surface thawing index, n_f is affected by many parameters such as the annual average temperature and snow depth [22]; and I_t and I_f are the air thawing and freezing indices, respectively, calculated by accumulating daily positive and negative air temperatures.

Given the complexity and difficulty in obtaining the n-factors, this study uses an earlier version of the TTOP model. The model calculates the $MAGT$ through the surface freeze-thaw index. The formula is as follows:

$$MAGT = \frac{\left(k_t / k_f \times TDD\right) - FDD}{P} \quad (2)$$

where TDD and FDD are the surface thawing degree-days and freezing degree-days, respectively, calculated directly from LST. This modification directly uses surface degree-days to compute the $MAGT$, thereby circumventing the complexity and potential inaccuracy associated with estimating the n-factors. It is generally believed that there is permafrost in the area where $MAGT$ is less than 0 °C.

2.2. Quantile Mapping Model

Quantile Mapping (QM) is a statistical downscaling method. At present, it has been widely used in the deviation correction of climate model data [32–34]. Its core principle involves calculating the empirical cumulative distribution functions (CDFs) for historical climate model data and corresponding observational data pixel by pixel and then establishing a mapping relationship between these two CDFs. Compared to other bias-correction methods like the Delta method, QM better preserves spatial heterogeneity and, with longer

training data series, effectively handles extreme climate events. For the air temperature variable in this study, we constructed pixel-wise observational CDFs (F_{obs}) and model CDFs (F_{mod}). The mapping function between low-resolution and high-resolution data is established as:

$$X_{high} = F_{obs}^{-1}\left(F_{mod}\left(X_{gcm}\right)\right) \quad (3)$$

where X_{gcm} is the future low-resolution data from the Global Climate Model. Within the mapping function, X_{gcm} serves as the input variable. Its quantile in the historical model CDF is computed, and this quantile is then used in the inverse CDF^{-1} of the historical observations to derive the corrected high-resolution value X_{high}. This process corrects the bias between low-resolution and high-resolution data, mapping the low-resolution data to high-resolution space based on historical statistical relationships.

2.3. Random Forest Regression Model

Land surface temperature (LST) is the most critical input parameter for the TTOP model, making the method of obtaining LST data crucial. In this study, MODIS_LST data were selected as the original data to simulate and predict the permafrost on the TP, and this data was also the initial output data for training the Random Forest regression model. The Terra satellite and Aqua satellite used to collect MODIS data were put into use after entering the 21st century. Therefore, the Random Forest regression model was selected to simulate the land surface temperature, and the land surface temperature before the 21st century (1979–2002) was obtained. The China Meteorological Forcing Data set (CMFD, 1979–2018) is the main input data set for model training, and other land surface factors (DEM, ground freezing thermal conductivity, ground melting thermal conductivity, month) are also used as input data. The monthly generated data of China's 1 KM surface temperature (MODIS_MODLT1M_LST, 2003–2014; MODIS_MYDLT1M_LST, 2003–2014) is the main output data for model training. The data of 2013 and 2014 were used to verify the training results to ensure that the model has a certain extrapolation ability. Random Forest (RF), an ensemble learning algorithm proposed by Breiman [35], builds multiple decision trees and combines their predictions, making it particularly suitable for handling high-dimensional features and nonlinear relationships. This study adopted the RF algorithm for LST simulation to address the lack of historical LST data. After multiple tuning sessions, the optimal model parameters were selected as follows: the number of trees was set to 200 to ensure sufficient predictive capability while avoiding excessively long training times; the maximum tree depth was limited to 15, and the minimum samples required to split a node was set to 5. These parameters jointly controlled the complexity of individual trees to prevent overfitting. The overall structure of this study is shown in Figure 2. The yellow box in Figure 2 contains the input data and output results of QM. The green box contains the input data and output results of the RF; the blue box shows the core model for simulating permafrost, the TTOP model, the input data are TDD and FDD, as well as k_t and k_f, which are represented by blue arrows.

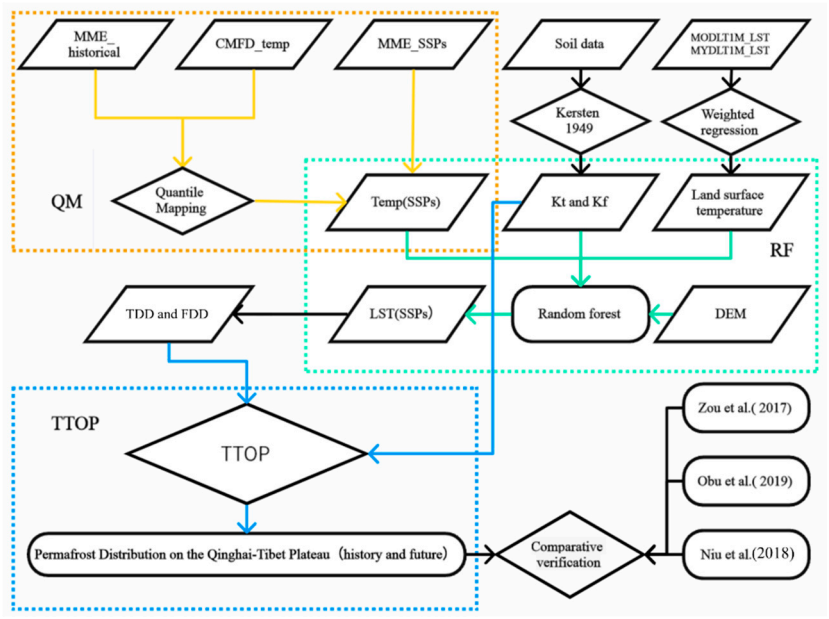


Figure 2. Structure of this study. (The results for comparative verification come from Zou et al. [12], Obu et al. [36] and Niu et al. [37]).

2.4. Data

2.4.1. Historical Data

The near-surface air temperature data for the historical period were obtained from the China Meteorological Forcing Dataset (CMFD1.6). This datasets was provided by the National Tibetan Plateau/Third Pole Environment Data Center (http://data.tpdc.ac.cn, accessed on 1 September 2025.). This dataset is specifically designed for meteorological and ecological studies in China, featuring long-term, high-resolution data [38,39]. The selected data specifications were monthly temporal resolution, covering 40 years (1979–2018) and a horizontal spatial resolution of 0.1°. This dataset served as the primary observational data for simulating historical permafrost distribution on the TP. The data set was also the high-resolution output in QM model training and the air temperature input in RF regression model training. For the historical period, CMFD through the RF regression model simulated LST from 1979 to 2018, which was then input into the TTOP model to simulate TP permafrost distribution.

LST data were primarily used to calculate the surface freezing and thawing indices, which were direct inputs to the TTOP model. Therefore, the accuracy of LST data directly influences the permafrost simulation results. This study selected MODLT1M_LST and MYDLT1M_LST data as historical LST sources. This data set was provided by the Geospatial Data Cloud site, Computer Network Information Center, Chinese Academy of Sciences. (http://www.gscloud.cn, accessed on 1 September 2025). These products are derived from MOD11C3 and MYD11C3 data collected by the Terra and Aqua satellites, respectively. The data have a monthly temporal resolution, cover 12 years (2003–2014), and have a horizontal spatial resolution of 1 km. The land surface temperature is obtained by taking a weighted average of day and night data—the weights refer to the research results of Zou et al. [12] The resulting equation converts the four MODIS LST bands (day and night from Terra and Aqua) into an estimate of ground surface temperature (GST), not the original MODIS skin temperature. When used as the dependent variable for RF regression model training, the spatial resolution was resampled to match the CMFD resolution (0.1°) using bilinear interpolation. When used for simulating TP permafrost distribution and comparing with results from other studies, the data were resampled to the resolution of those other studies

to facilitate model validation and ensure methodological feasibility. The same is true of the treatment of other researchers [25].

2.4.2. Future Projection Data

Future forecast data came from six models in the Coupled Model Intercomparison Project Phase 6 (CMIP6). This project provides very authoritative future climate prediction data [40]. This study selected the following six modes: ACCESS-CM2, CanESM5, FGOALS-f3-L, MIROC6, MRI-ESM2-0, and NorESM2-MM (variable is tas). These models provide historical data and projections under four different socioeconomic and climate change scenarios: SSP1–2.6, SSP2–4.5, SSP3–7.0, and SSP5–8.5. By calculating the temporal and spatial correlation between the historical data from these models and the CMFD data, it is found that these six models have good simulation ability in the TP region. Subsequently, the six models were weighed and averaged based on their correlation coefficients, and the multi-model ensemble mean (MME) demonstrated better performance compared to individual models. Many studies based on CMIP6 have confirmed that the performance of MME is superior to a single mode in all aspects [41,42]. The MME data was mainly used to train the QM model and simulate the distribution of TP permafrost in the future. The data have a monthly temporal resolution, cover 86 years (2015–2100), and their original spatial resolutions range from 1.0° to 1.25°. During the ensemble averaging process, the spatial resolution of all six models was unified to 0.1° via bilinear interpolation. For the prediction of future permafrost, the QM model was used to reduce the MME data to 0.1°. The bilinear difference method was used to increase the data resolution difference to 1 km to improve the data's accuracy. Then, the RF regression model was applied to simulate future LST under the four scenarios. Finally, the TTOP model was used to obtain the results.

2.4.3. Soil Thermal Conductivity

The soil thermal conductivity used as an input parameter was simulated based on the soil type distribution across the TP and the empirical model from Kersten [43]. Required data included soil dry bulk density and soil moisture content.

For unfrozen sandy soil:

$$k_t = 0.1442 \times (0.7 \times log\omega + 0.4) \times 10^{0.6243 \times \rho} \quad (4)$$

For frozen sandy soil:

$$k_f = 0.001096 \times 10^{0.8116 \times \rho} + 0.00461\omega \times 10^{0.9115 \times \rho} \quad (5)$$

For unfrozen fine-grained soil:

$$k_t = 0.1442 \times (0.9 \times log\omega - 0.2) \times 10^{0.6243 \times \rho} \quad (6)$$

For frozen fine-grained soil:

$$k_f = 0.001442 \times 10^{1.373 \times \rho} + 0.01226\omega \times 10^{0.4994 \times \rho} \quad (7)$$

where ω is soil moisture content (%) and ρ is soil dry bulk density (g/cm^3). Using these data and formulas, the thermal conductivities of frozen and thawed soils are calculated. In this study, soil thermal conductivity served both as an input parameter for the TTOP model and as an important feature in the RF regression model training.

3. Results

3.1. Historical Permafrost on the Tibetan Plateau (1979–2018)

The interannual variations of the mean annual air temperature and the RF-predicted annual mean LST over the TP from 1979 to 2018 are shown in Figure 3. The figure shows that LST is generally higher than near-surface air temperature during the same period, and both exhibit a gradual warming trend. The rate of LST increase is slightly lower than that of air temperature, indicating a somewhat moderated response of the land surface to climate warming compared to the air. The overall trends of air temperature and LST are similar. As LST directly influences the degradation rate of TP permafrost, it is necessary to study its evolution under different SSP scenarios.

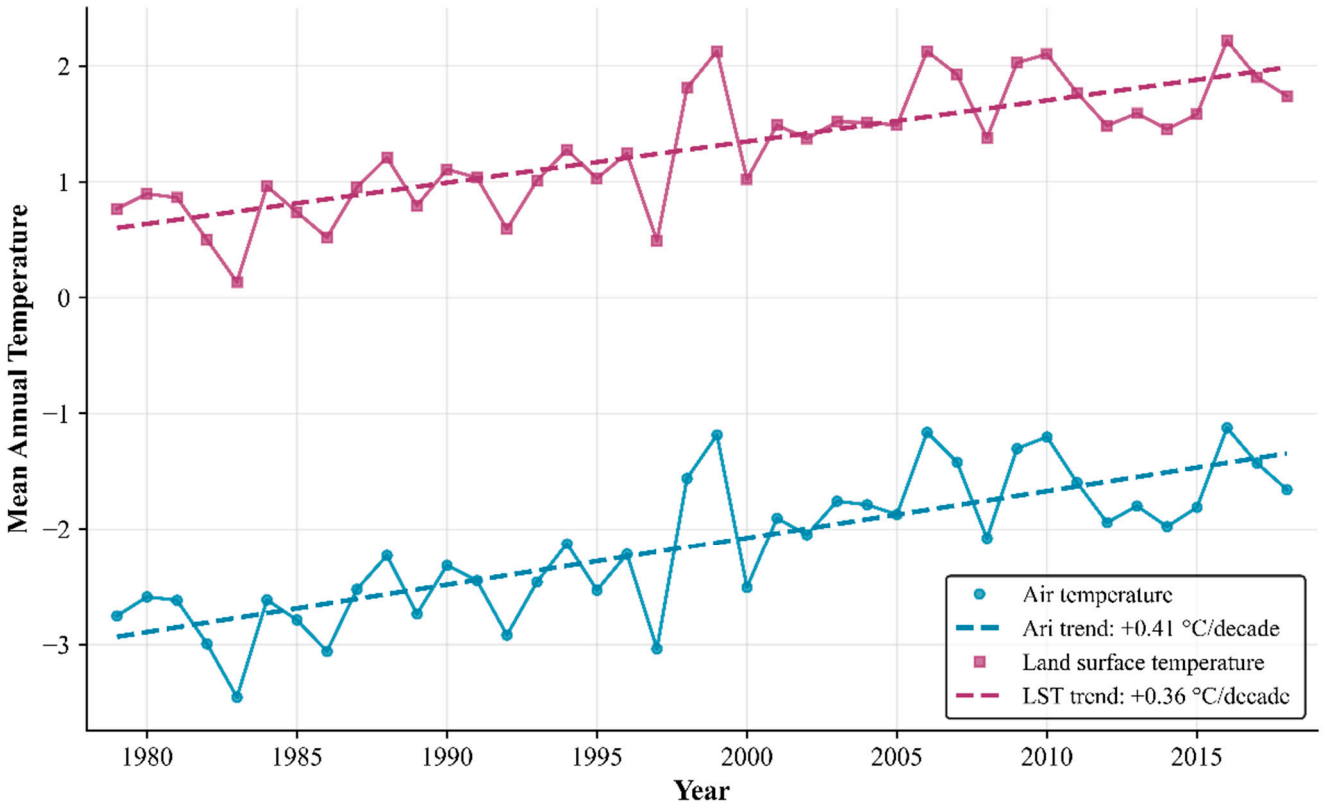


Figure 3. Interannual variations of mean annual air temperature and land surface temperature during the historical period.

Figure 4 displays the spatial distribution of decadal mean air temperature changes for four periods within 1979–2018. The temperature change for 1979–1988 referenced against the mean annual temperature of 1979, the earliest year in our dataset. The figure shows minor temperature fluctuations in the first two periods, with some areas of the TP even experiencing cooling. The magnitude of temperature change in these first two periods mainly was within 1 °C, not exceeding 2 °C. Starting from the third period, temperatures began to rise sharply, with many regions warming, and increases exceeding 5 °C in some areas. Compared to the third period, the warming in the fourth period moderated but remained on an upward trend. The average temperature changes for the four periods from 1979 to 2018 were −0.009 °C, 0.32 °C, 0.66 °C, and 0.19 °C, respectively.

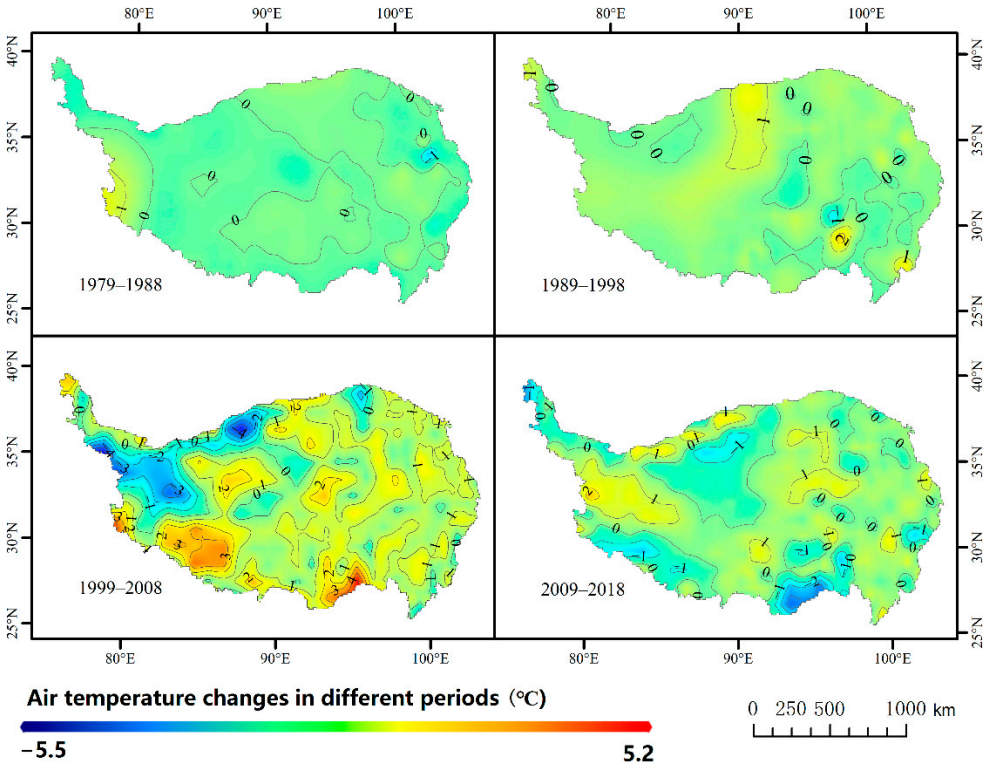


Figure 4. Spatial distribution of air temperature changes over the Tibetan Plateau during the historical period.

Figure 5 shows the spatial distribution of permafrost on the TP for the four historical periods. The permafrost is determined where the *MAGT* calculated by TTOP is lower than 0 °C; other areas are classified as seasonally frozen soil. The corresponding permafrost areas are listed in Table 1. Permafrost on the TP is primarily distributed in the Kunlun Mountains of the Qiangtang Plateau, the Gangdise Mountains in the south, the Qilian Mountains in the northeast, and the Tanggula and Hengduan Mountains in the southeast. From 1979 to 2018, permafrost continuously degraded, shrinking from 1.427 million km^2 during 1979–1988 to 1.118 million km^2 during 2009–2018. This signifies a loss of over 20% of the permafrost present in 1979. Table 1 indicates an average historical degradation rate of 1.03 × 10^4 km^2/a from 1979 to 2018. The most significant degradation occurred between 1989–1998 and 1999–2008, with approximately 18.27 × 10^4 km^2 of permafrost disappearing. The permafrost degradation rate aligns with the rate of temperature increase. Degradation primarily occurred at the margins of the permafrost distribution, with the most severe degradation observed in the southernmost part of the Qiangtang Plateau, north of the Gangdise Mountains, and near the headwaters of the Yarlung Zangbo River, Za Qu, Lancang River, Tongtian River, and Yellow River.

Table 1. Changes in permafrost area on the Tibetan Plateau during the historical period (Unit: 10^4 km^2).

	1979–1988	1989–1998	1999–2008	2009–2018
permafrost	142.73	135.68	117.41	111.88
seasonal frozen soil	118.25	125.29	143.56	149.10

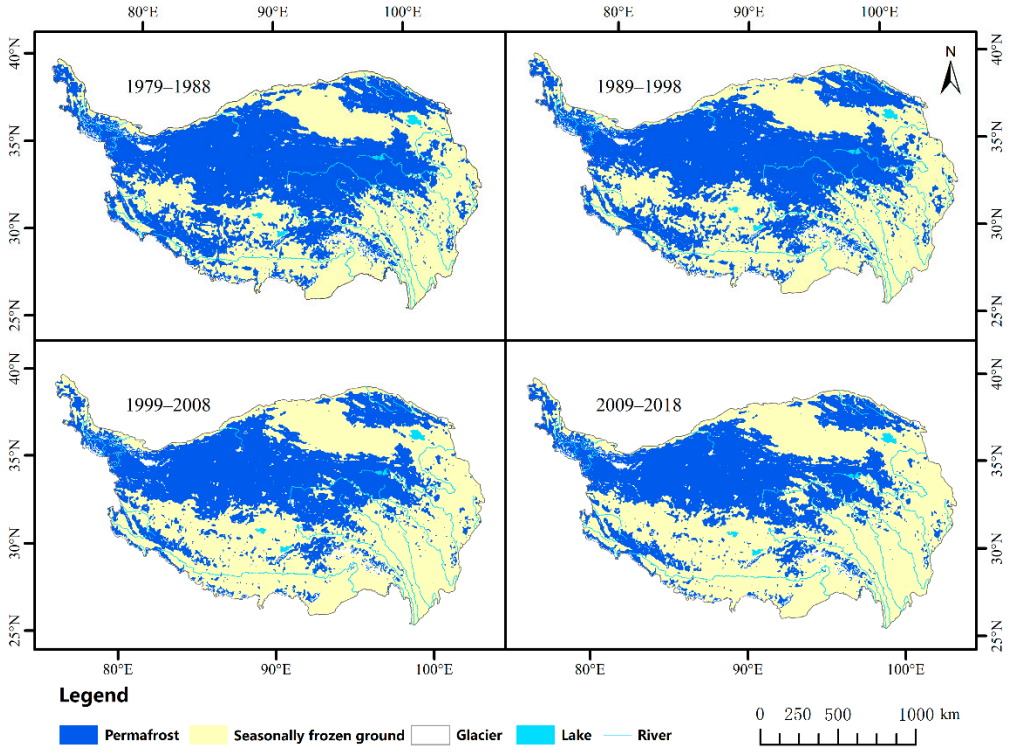


Figure 5. Spatial distribution of permafrost on the Tibetan Plateau during the historical period.

3.2. Future Projections of Permafrost on the Tibetan Plateau

Future projections (2019–2100) of TP permafrost are based on the multi-model ensemble data from CMIP6 under four SSP scenarios. The future period is also divided into four intervals for study: 2019–2040, 2041–2060, 2061–2080, and 2081–2100, each spanning approximately 20 years. The temperature change in 2019–2040 is compared with the baseline in 2009–2018, and the subsequent period is compared with the previous period. Under all four future scenarios, air temperatures continue to rise persistently (Figure 6). Under SSP1–2.6, warming is slowest and shows a decelerating trend, with an average increase of 1.0 °C in 2019–2040, but only 0.04 °C in 2081–2100. This suggests that a highly sustainable economic pathway can effectively mitigate warming, potentially stabilizing temperatures in the future. Under SSP5–8.5, warming is most intense and exhibits an accelerating trend, with an average increase of 0.95 °C in 2019–2040, reaching 1.64 °C in 2081–2100, far exceeding the historical rate of 0.41 °C/decade. Spatially, warming is more pronounced in the northern TP, generally increasing from south to north. The rate of temperature increase will be slowed down under SSP1–2.6 and SSP2–4.5, and the mitigation effect under the SSP1–2.6 scenario is the most obvious. The rate of temperature rises under SSP3–7.0 and SSP5–8.5 scenarios will gradually increase, and the temperature rise under the SSP5–8.5 scenario is the most severe.

Figure 7 shows the evolution of permafrost spatial extent on the TP under different SSPs. Permafrost degrades under all four scenarios, with the degradation rate strongly correlated with the magnitude of warming: slowest under SSP1–2.6, and increasing through SSP2–4.5 and SSP3–7.0 to SSP5–8.5. Table 2 lists the areas of permafrost and seasonal frozen soil under different SSPs. Under SSP5–8.5, by 2081–2100, the permafrost area on the TP is projected to be only 19.71 $\times$ 10^4 km^2, meaning approximately 92.17 $\times$ 10^4 km^2 of the permafrost present in 2009–2018 will have degraded, leaving just 17.6% of the baseline area. Correspondingly, under SSP1–2.6, SSP2–4.5, and SSP3–7.0, permafrost area by the end of the century is projected to be 79.9%, 62.43%, and 30.9% of the current (2009–2018) area, respectively. Spatially, under SSP1–2.6 and SSP2–4.5, permafrost degradation patterns

are like the historical period, primarily occurring in the southern and eastern parts of the Qiangtang Plateau, near the Qilian Mountains, and along major river basins. Under SSP3–7.0 and SSP5–8.5, degradation is exceptionally severe, especially toward the end of the century, where permafrost near the Gangdise Mountains virtually disappears. The remaining permafrost is distributed only in the northwest of the Qiangtang Plateau and near the Qilian Mountains.

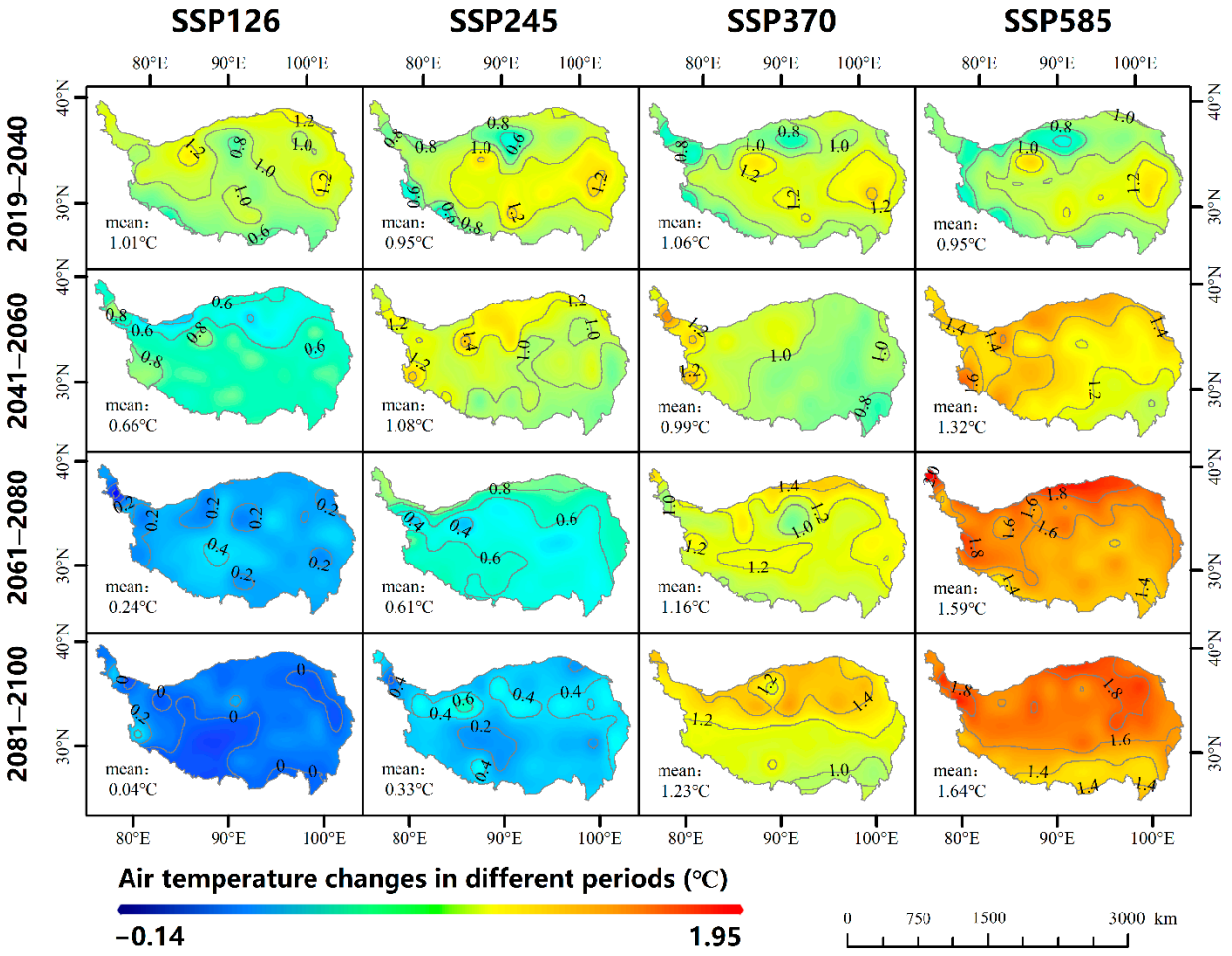


Figure 6. Projected temperature increases over the Tibetan Plateau under different SSPs.

Table 2. Projected changes in permafrost area on the Tibetan Plateau under different SSPs (Unit: 10^4 km^2).

SSPs	Frozen Soil Types	2019–2040	2041–2060	2061–2080	2081–2100
SSP1–2.6	Permafrost	102.88	92.70	89.20	89.38
	Seasonal frozen soil	158.10	168.28	171.78	171.60
SSP2–4.5	Permafrost	102.39	86.81	76.83	69.85
	Seasonal frozen soil	158.59	174.17	184.14	191.13
SSP3–7.0	Permafrost	100.94	80.41	58.50	34.52
	Seasonal frozen soil	160.04	180.57	202.47	226.45
SSP5–8.5	Permafrost	99.22	73.08	45.18	19.71
	Seasonal frozen soil	161.76	187.89	215.79	241.27

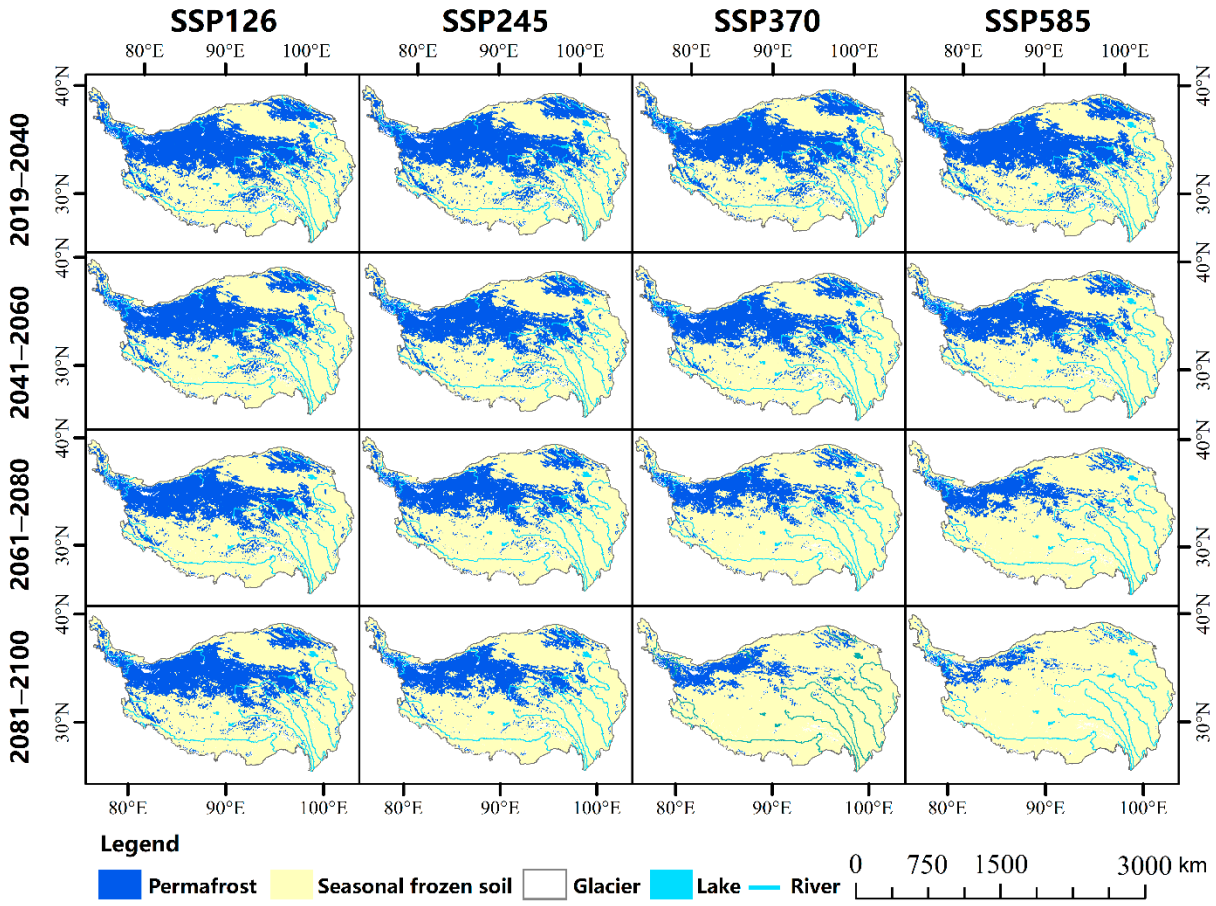


Figure 7. Evolution of permafrost distribution on the Tibetan Plateau under different SSPs.

3.3. Sensitivity Analysis

To assess the robustness of our projections and to explore the spatial heterogeneity of permafrost degradation, we conducted two additional sensitivity analyses: (i) elevation-zone breakdown to examine altitudinal controls and (ii) perturbation of the soil thermal conductivity ratio (k_t/k_f) to evaluate parametric uncertainty.

3.3.1. Elevational Differentiation of Permafrost Degradation

To investigate the spatial heterogeneity of permafrost degradation, we divided the Tibetan Plateau into five elevation zones (<4000 m, 4000–4500 m, 4500–5000 m, 5000–5500 m, and >5500 m) based on the DEM. Table 3 presents the permafrost area (10^4 km^2) and its percentage within each zone for the historical period (2009–2018) and for the end of the 21st century (2081–2100) under four SSPs.

Table 3. Elevation-zone breakdown of permafrost area (10^4 km^2) and percentage of permafrost in the elevation zoning (%) on the Tibetan Plateau for the historical period (2009–2018) and for 2081–2100 under different SSP scenarios.

Elevation Zone	Historical	SSP1–2.6	SSP2–4.5	SSP3–7.0	SSP5–8.5
<4000 m	6.34 (8.69%)	4.05 (5.56%)	2.47 (3.38%)	0.63 (0.86%)	0.21 (0.28%)
4000–4500 m	17.54 (39.18%)	13.14 (29.36%)	9.23 (20.61%)	3.72 (8.30%)	1.62 (3.62%)
4500–5000 m	38.49 (47.43%)	32.82 (40.45%)	25.08 (30.91%)	9.53 (11.74%)	4.29 (5.29%)
5000–5500 m	40.70 (85.82%)	32.15 (61.75%)	26.69 (51.26%)	15.69 (30.13%)	9.38 (18.02%)
>5500 m	8.81 (89.04%)	7.12 (71.98%)	6.32 (63.89%)	4.93 (49.82%)	4.19 (42.31%)

In the historical period, permafrost is concentrated in high-altitude areas: More than 80% of the area above 5000 m is covered by permafrost., while the zone below 4000 m has only 8.7% permafrost coverage. This altitudinal gradient reflects the dominant control of temperature on permafrost distribution. Under future climate warming, permafrost degradation follows a clear elevation-dependent pattern. For the low elevation zone (<4000 m), the permafrost area shrinks from 6.34×10^4 km^2 historically to 0.21×10^4 km^2 under SSP5 8.5 (a loss of 96.7%), and the percentage drops to only 0.28%. In contrast, for the highest zone (>5500 m), the permafrost area decreases from 8.81×10^4 km^2 to 4.19×10^4 km^2 (−52.5%), with 42.3% of the zone still underlain by permafrost even under the most extreme warming scenario. Intermediate elevation zones show intermediate losses. Under the low-emission scenario SSP1 2.6, the losses are substantially moderated: the >5500 m zone retains 71.98% of its permafrost coverage and 5.56% of the area < 4000 m remains covered by permafrost.

This elevation-dependent analysis confirms that high-altitude regions act as refugia for permafrost under global warming, while low- and mid-elevation permafrost is highly vulnerable and is projected to largely disappear by 2100 under high-emission pathways. These findings have important implications for the spatial planning of infrastructure and for the assessment of climate change impacts on headwater catchments.

3.3.2. Sensitivity to Soil Thermal Conductivity Ratio

To evaluate the sensitivity of the TTOP model to uncertainties in soil thermal conductivity, we performed a perturbation analysis by scaling the ratio k_t/k_f (thawed to frozen thermal conductivity) by factors of 0.75 and 1.25 while keeping all other parameters unchanged. The simulations were conducted for the end of the 21st century (2081–2100) under the four SSPs. The resulting permafrost areas are summarized in Table 4.

Table 4. The sensitivity analysis was performed by scaling the thermal conductivity ratio k_t/k_f by ±25% for the period 2081–2100 (Unit: 10^4 km^2).

SSPs	Baseline	$k_t/k_f \times 0.75$	$k_t/k_f \times 1.25$
SSP1–2.6	89.38	113.45 (+26.9%)	69.05 (−22.7%)
SSP2–4.5	69.85	79.61 (+14.0%)	65.45 (−6.3%)
SSP3–7.0	34.52	42.76 (+23.9%)	15.93 (−53.9%)
SSP5–8.5	19.71	25.53 (+29.5%)	9.02 (−54.2%)

Under SSP1–2.6, the baseline permafrost area is 89.38×10^4 km^2. Reducing k_t/k_f by 25% increases the area by 26.9% to 113.45×10^4 km^2, whereas increasing it by 25% decreases the area by 22.7% to 69.05×10^4 km^2. This indicates moderate sensitivity when the remaining permafrost is extensive. In contrast, under the high-emission scenarios (SSP3–7.0 and SSP5–8.5), the sensitivity is substantially larger. Under the SSP5–8.5 scenario, the base area is 9.71×10^4 km^2. When k_t/k_f increases by 25%, the area decreases by 54.2% to 9.02×10^4 km^2. When k_t/k_f decreases by 25%, the area increases by 29.5% to 25.53×10^4 km^2. The asymmetric response reflects the fact that in a warm climate, the thawed thermal conductivity dominates the heat transfer, making the system more sensitive to increases than to decreases in the k_t/k_f. The high sensitivity under SSP5–8.5 implies that uncertainties in soil thermal properties could lead to a wide range of permafrost area estimates (9×10^4 km^2–26×10^4 km^2) for the most extreme warming pathway. Nevertheless, under all scenarios, the qualitative conclusion of progressive permafrost degradation remains robust: even in the most optimistic case (k_t/k_f reduced by 25% under SSP5–8.5), the remaining permafrost area (25.53×10^4 km^2) is only about one-quarter of the historical baseline (111.88×10^4 km^2 in 2009–2018). The parameter sensitivity analysis in Table 4

provides an interval reference for the possible permafrost region under the uncertainty of soil thermal properties. For example, under SSP5–8.5, the baseline permafrost area (19.71×10^4 km^2) varies from 9.02×10^4 km^2 to 25.53×10^4 km^2 when the thermal conductivity ratio k_t/k_f is perturbed by ±25%. The corresponding ranges of other SSP scenarios are also shown in Table 4. Therefore, the area estimation in Table 2 should be regarded as the central value, and the actual permafrost range is reasonably within the interval obtained by the disturbance of soil thermal conductivity.

3.4. Validation of the TTOP Model

Given the modification in calculating the TDD and FDD input parameters for the TTOP model, it was essential to validate the feasibility of this approach before the primary analysis. This study selected existing permafrost distribution results for the TP from Zou et al. [12], Obu et al. [36], and Niu et al. [37]. Among them, Zou et al. and Obu et al. used the TTOP model while Niu et al. employed a decision tree method based on multi-source remote sensing data. The simulation results from our TTOP model for the corresponding period were overlaid and analyzed against these references. By counting pixels correctly classified as permafrost and non-permafrost and those misclassified, a confusion matrix was derived, and the Kappa coefficient was calculated using the following formula:

$$k = \frac{(a_1 + a_2)n^2 - [(a_1 + b_1)(a_1 + b_2) + (a_2 + b_1)(a_2 + b_2)]}{n^2 - [(a_1 + b_1)(a_1 + b_2) + (a_2 + b_1)(a_2 + b_2)]} \quad (8)$$

where a_1 is the number of pixels correctly identified as permafrost by our method, a_2 is the number correctly identified as non-permafrost, b_1 is the number misclassified as permafrost, b_2 is the number misclassified as seasonal frozen soil, and n is the total number of pixels in the region. The calculated Kappa coefficients were k_a = 0.758 (vs. Zou [12]), k_b = 0.769 (vs. Obu [36]), and k_c = 0.752 (vs. Niu [37]), indicating close agreement with other studies and confirming the feasibility of the model modification. The overlay results are shown in Figure 8.

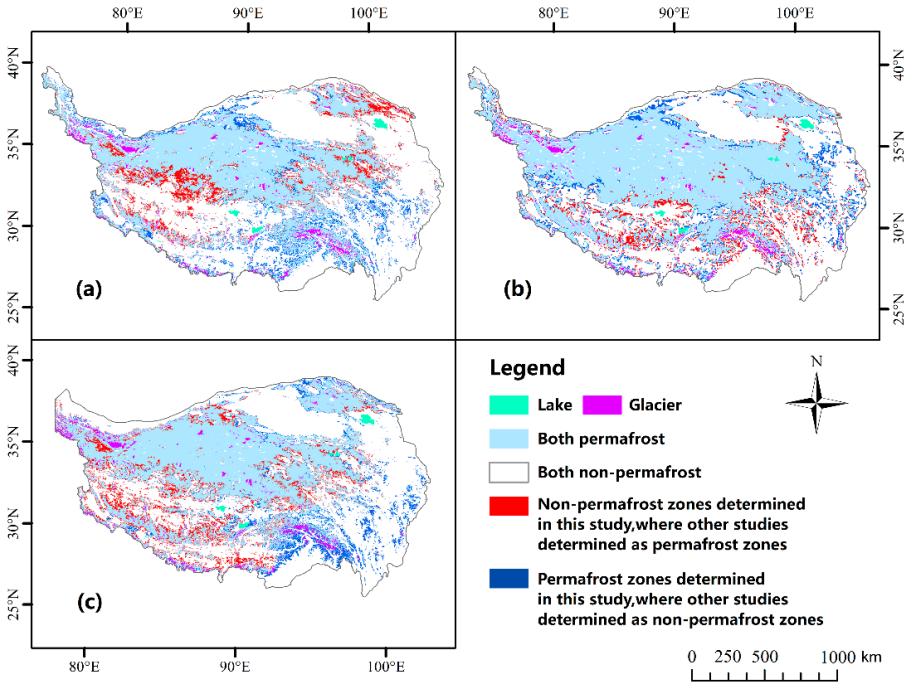


Figure 8. Comparison and validation against existing studies: (**a**) comparison with the results of Zou et al. [12]; (**b**) comparison with the results of Obu et al. [36]; (**c**) comparison with the results of Niu et al. [37].

To directly evaluate the performance of the TTOP model in simulating the permafrost thermal regime, we collected 132 measurements of *MAGT* at 10 m depth from 12 boreholes located along the G109 National Highway corridor on the TP, spanning the period 2004–2018 [44]. These observations provide a benchmark for model validation. Figure 9a presents the scatterplot of simulated versus observed *MAGT*. The root mean square error (RMSE) is 0.724 °C. Notably, 90% of the validation points fall within the ±1 °C error margin.

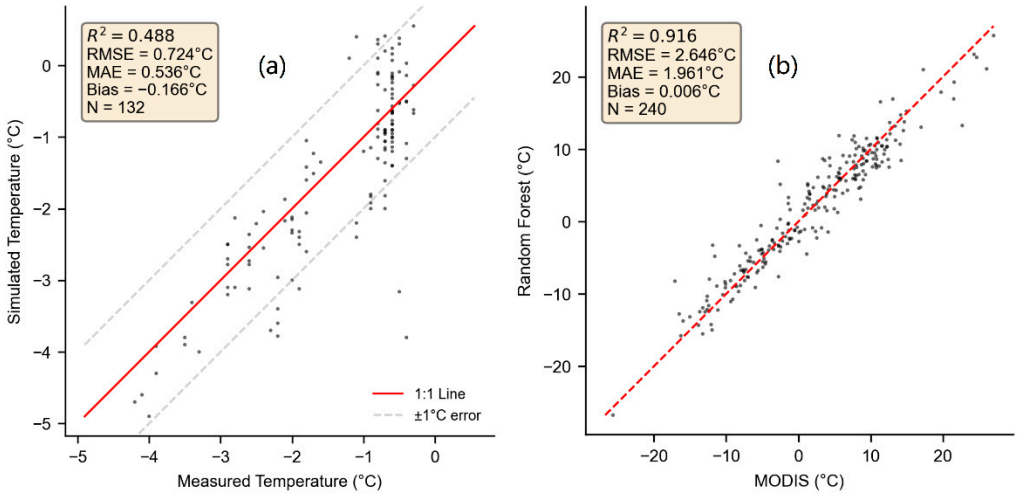


Figure 9. Comparison between simulated *MAGT* with the observed *MAGT* (**a**) Accuracy assessment of the Random Forest regression model (**b**).

The validation statistics are comparable to those reported in previous TTOP-based permafrost mapping studies of the Tibetan Plateau [12,24,25]. The model exhibits a slight underestimation of *MAGT* (bias = −0.166 °C). Nevertheless, these results confirm that the model can reproduce the observed permafrost thermal regime with acceptable accuracy, providing a solid basis for subsequent historical and future permafrost projections.

3.5. Performance of the Quantile Mapping Model

This study used 15 years (2000–2014) of CMFD data as the high-resolution observational reference and 15 years (2000–2014) of multi-model ensemble (MME) data as the initial low-resolution data for model training. The model was trained monthly to best preserve the unique spatial distribution characteristics of air temperature for each month. To test the accuracy of the model, some data was retained as the test set, evaluated using the coefficient of determination (R^2), mean error (bias), and root mean square error (RMSE). This study compared QM and the Delta method for downscaling 2014 climate model data and found QM results superior in terms of mean bias, mean absolute error, and RMSE (the Delta method used year 2000 data for bias calculation). The evaluation results are shown in Figure 10.

Statistical calculations showed that most errors ranged between 0 °C and 2 °C, with a mean error of −0.28 °C and an RMSE of 1.04 °C, indicating a slight overall undervalued trend in the downscaling model. In contrast, the accuracy of the Delta method is not as good as that of QM, indicating that QM has better performance in the downscaling of climate model data. A known characteristic of QM is its tendency to regress extreme values toward the mean, slightly underestimating high values and overestimating low values. For this study, since the critical threshold for permafrost presence is the 0 °C TTOP isotherm, a slight underestimation of high values and overestimation of low values does not significantly impact the final permafrost classification. Overall, the QM method is an optimal choice for resolution enhancement when auxiliary data are scarce. The future

climate model data after mapping can better represent spatial details and future trends in air temperature.

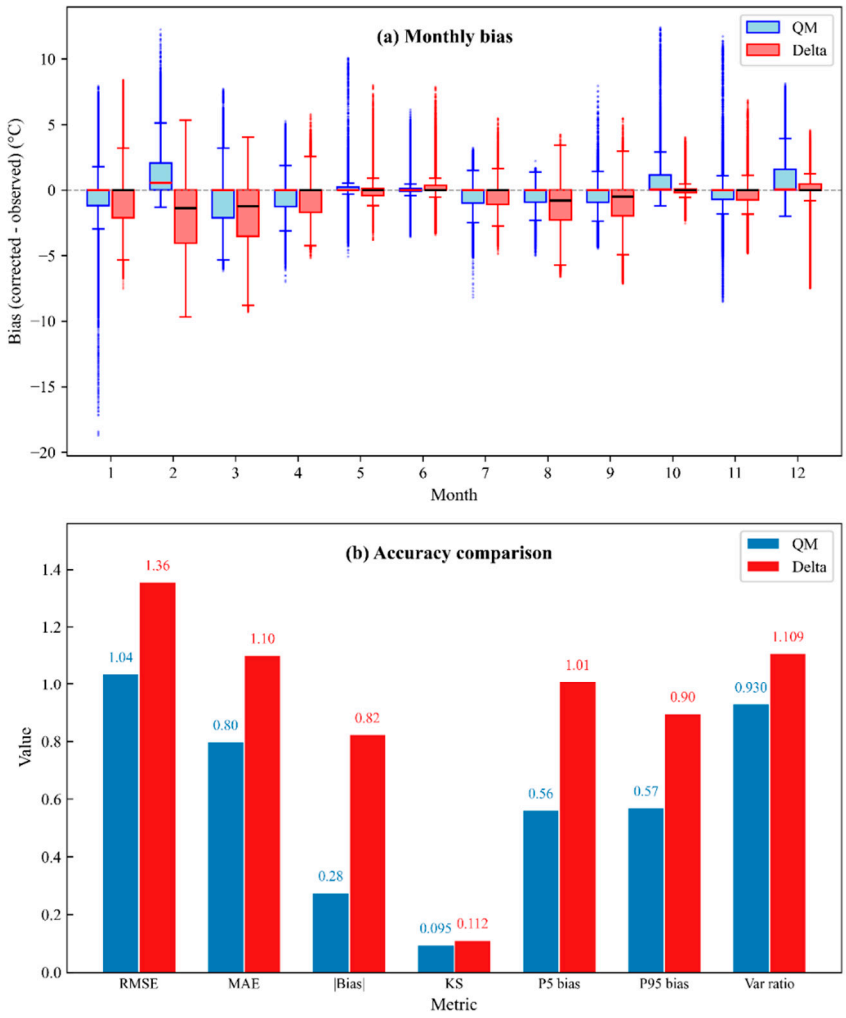


Figure 10. The distribution of residuals of QM and Delta downscaling methods in 12 months (**a**) and the comparison of accuracy indexes of QM and Delta downscaling methods (**b**).

3.6. Performance of the Random Forest Regression Model

In applying the TTOP model, this study used the conventional process, calculating land surface freezing/thawing indices through LST. The temperature data, which is easy to obtain, is taken as the independent variable, the soil thermal conductivity and DEM obtained by Kersten (1949) [43] empirical model are taken as the important features, and the surface temperature data, which is difficult to obtain, is taken as the output variable. Before analysis, all data were resampled to the same spatial resolution using bilinear interpolation, and dynamic data (air and land surface temperature) were aligned to the same temporal resolution. The accuracy of the model was evaluated using the same indicators as the QM model (Figure 9b).

Statistical calculations indicated that most errors in the regression model were within 3 °C, with a mean error of 0.006 °C and an RMSE of 1.961 °C, suggesting a robust simulation capability for LST. The R^2 value was 0.916, showing that the model reliably predicts LST corresponding to most air temperature values, providing solid data support for subsequent calculation of freezing/thawing indices and simulation of TP permafrost distribution. To evaluate the extrapolation risk under future climate conditions, we compared the monthly air temperature of the SSP5–8.5 scenario with the corresponding monthly training ranges.

The training ranges vary seasonally, with the coldest minimum in January (−35.18 °C) and the warmest maximum in August (32.23 °C). Under SSP5–8.5, only 1.07% of the valid monthly grid cells exhibit air temperatures outside the corresponding monthly training envelope. The highest monthly extrapolation ratio is 1.21% (October). These results demonstrate that the RF model is required to extrapolate only for a negligible fraction of the study area, even under the most extreme emission scenario. Therefore, extrapolation-induced errors do not compromise the reliability of our permafrost projections.

4. Discussion

4.1. Contributions of This Study

To contextualize the findings, two recent TTOP based permafrost projection studies over the Tibetan Plateau were selected for comparison: Li et al. [24] and Zhao et al. [25]. Although all three studies employ the TTOP model driven by CMIP6 multi-model ensembles, there are substantial differences in methodology, forcing data, and parameterization, which lead to divergent projections. Li et al. [24] used the classical TTOP formulation with n-factors derived from air temperature and snow depth, applying the Delta downscaling method to future climate data. Zhao et al. [25] also rely on the Delta method and use land-cover-specific n-factors and thermal conductivity ratios (r_k), assuming they remain constant in the future. In contrast, the present study introduces two innovations: LST from MODIS and RF-simulated LST is directly used to calculate surface freezing/thawing degree-days, thereby circumventing the uncertain estimation of n-factors. Also, QM is employed instead of the Delta method for downscaling.

Li et al. [24] report an average permafrost area of 1.34×10^6 km^2 for the current period (2001–2020), whereas Zhao et al. [25] estimate 1.03×10^6 km^2 for 2010–2018. The historical simulation in this study (2009–2018) yields 1.12×10^6 km^2, which lies between these two estimates. The historical degradation rate in this study (1.03×10^4 km^2/a, corresponding to a loss of more than 20% from 1979–1988 to 2009–2018) is comparable to the 7.74×10^3 km^2/a reported by Li et al. [24] for 1975–2006, although the rate in this study is slightly higher, possibly due to the longer and more recent warming period considered.

The projected degradation rates of TP permafrost under SSP1–2.6, SSP2–4.5, SSP3–7.0, and SSP5–8.5 are 0.14×10^4 km^2/a, 0.49×10^4 km^2/a, 0.93×10^4 km^2/a, and 1.16×10^4 km^2/a, respectively. By 2100, approximately 20.1%, 37.57%, 69.1%, and 82.4% of the permafrost present in 2009–2018 is projected to be lost. Compared to the results of Li et al. [24]—a potential reduction of 16.23% (SSP1–2.6) and 35.19% (SSP5–8.5) by mid-century relative to 2020, and 18.80% (SSP1–2.6) and 63.28% (SSP5–8.5) by the end of the century—our estimates are generally higher, representing a more aggressive projection. Compared to the results of Zhao et al. [25]—projecting permafrost area reduction to 75%, 49%, 29%, and 17% of the current area (2010–2018) under SSP1–2.6, SSP2–4.5, SSP3–7.0, and SSP5–8.5 by the end of the century, equivalent to losses of 25%, 51%, 71%, and 83%—our estimates are generally lower. These differences stem from methodological variations in calculating future parameters and the selection of future climate model data. The future evolution of TP permafrost is highly complex. Validation against historical data has proven the method sound. Therefore, this study, through methodological improvements, provides a more reliable projection, offering valuable references for engineering construction on the TP.

The projected permafrost degradation has profound implications for sustainable development on the Tibetan Plateau. It affects the stability of critical infrastructure (e.g., the Qinghai–Tibet Highway and Railway), the seasonality of water supply from headwater catchments, and the integrity of alpine ecosystems. Therefore, incorporating permafrost dynamics into regional sustainability assessments is essential for climate-resilient planning.

4.2. Overall Model Assessment

4.2.1. Advantages and Limitations of the TTOP Model

Selecting a model suited to the study region is crucial before conducting research. Generally, models with more parameters and greater complexity can yield more accurate results. However, because permafrost is often distributed in extremely cold areas with high altitude and high latitude, the available data are scarce. The TTOP model requires only surface freezing/thawing indices and soil thermal conductivities in frozen and thawed states to simulate contemporary permafrost distribution. The soil thermal conductivity is directly related to the soil type. The average distribution of permafrost in the TP in the corresponding period can be obtained only by inputting the calculated freeze-thaw index. In addition, the permafrost can be classified into different stability grades by classifying the calculated $MAGT$ according to a certain interval [45].

Li et al. [24] noted that the n-factor (n_t) correcting between surface and air freezing indices in future climate scenarios is a variable that changes with vegetation cover. Under future thawing and warming conditions, vegetation tends to grow rapidly, forcing researchers to assume n_t as a constant. In this study, although n_t and n_f were omitted, the RF model implicitly captured the nonlinear relationship between these n-factors and topographic, soil, and air temperature variables. Therefore, the model is not simplified. RF is particularly adept at handling complex, nonlinear regression problems with multiple features. Its advantages include simplicity, efficiency, and a mechanism that reduces model variance through averaging predictions, performing significantly better than other linear models [46]. The essence of adjusting the atmospheric freeze-thaw index by the n-factor is to make a linear transformation of the atmospheric freeze-thaw index. Therefore, the machine learning-driven method is superior to the traditional method. Transforming the relationship from surface/air degree-day ratios to a dynamic LST-air temperature conversion under varying elevation, topography, and soil conditions undoubtedly increases model flexibility. Applying this mapping relationship to the future period can effectively reduce the errors caused by future changes in n_t, such as vegetation growth. Figure 8 shows the comparison between the results of the TTOP model without the correction factor and the results of the TTOP model with the correction factor. That the Kappa coefficients are all above 0.75 confirms the feasibility of this adjustment.

The dynamic inputs for the TTOP model are air or surface freezing/thawing indices, requiring statistical accumulation of positive and negative temperatures over a period. Consequently, the permafrost distribution derived from TTOP represents an average state over a year or period and cannot capture transient freeze-thaw dynamics. Furthermore, while air and land surface temperatures are dominant factors, many other elements significantly influence permafrost stability. Soil properties affect degradation, and geological strata strongly influence the degradation process. Reducing snow depth from 0.7 m to 0.1 m can delay permafrost thaw by over 140 years [47]. Similarly, permafrost degradation is closely related to vegetation coverage. Thawing ground increases soil moisture, and rising temperatures promote rapid vegetation growth [48]. Higher vegetation coverage provides greater insulation, indirectly raising ground temperature and accelerating permafrost degradation. Solar radiation plays a key role in the surface energy balance; increased radiative input leads to ground warming and intensified permafrost degradation. Aside from solar radiation, evapotranspiration and precipitation are also critical factors [49]. These factors are not considered in the TTOP model. Permafrost degradation is an extremely complex process. While we cannot ignore these influences, the common goal among researchers is to obtain the most realistic simulations possible with available data.

4.2.2. Advantages of the Quantile Mapping Model

Unlike the commonly used Delta method in previous studies, this study employed QM for downscaling. QM can more effectively correct the systematic bias in climate models and is particularly skilled at preserving spatial details and extreme event information in future climate projections, thereby providing more reliable, higher-resolution future permafrost estimates and reducing uncertainty introduced by the downscaling method [50]. QM is a more advanced bias-correction method, and it is one of the statistical downscaling methods. It works by statistically deriving the empirical CDFs of historical climate model data and high-resolution observational data used as the downscaling target, then establishing a mapping relationship between these two functions. This method goes beyond correcting the mean bias per pixel, flexibly adjusting based on the historical data distribution to better match the actual distribution, which has been widely used in meteorology. Another advantage of QM is that it requires only historical data for training, without needing other auxiliary data for correction.

4.3. Limitations of This Study

The primary limitation lies in the application of the Random Forest regression model. The RF model in this study treated various topographic and soil factors as static data, which is unrealistic. Under persistent future warming, accompanied by permafrost thaw, ground surface heave or subsidence may occur; Mahanta et al. [51] detailed the mechanism of permafrost degradation-induced subsidence in the Indian Tethyan Himalayas. Furthermore, with ground warming, soil moisture content, thermal conductivity, and other soil factors would inevitably be affected. Therefore, subjectively assuming these auxiliary data as static variables is unreasonable. However, among all input data for LST simulation, air temperature has a strong correlation with LST and accounts for over 90% of the importance in the regression model. The assumption that soil and topographic factors are constant will certainly affect the accuracy of the results, but the ability to influence them is limited.

The thermal conductivity of the ground in frozen and thawed states is not only an input feature for RF but also a crucial parameter for the TTOP model. Assuming it is constant will undoubtedly introduce errors. This static assumption is particularly critical under high-emission scenarios. As shown in Table 4, a ±25% perturbation of k_t/k_f changes the projected permafrost area under SSP5–8.5 from 9.02×10^4 km^2 to 25.53×10^4 km^2, demonstrating that the uncertainty in soil thermal properties can substantially affect the absolute area, even though the qualitative degradation trend remains robust. However, we, like other related researchers, currently lack a method to accurately predict the dynamic changes of soil thermal conductivity in the future, necessitating this assumption [24,25].

We acknowledge that the TTOP model, as used in this study, does not strictly distinguish between the temperature at the permafrost table (TTOP) and the $MAGT$ at the depth of zero annual amplitude. In permafrost science, $MAGT$ typically refers to the temperature at 10–20 m depth where seasonal fluctuations have disappeared, while TTOP is specifically the temperature at the permafrost surface [15,52]. In our study, the simulated ground temperatures were validated against borehole measurements at 10 m depth (Figure 9a), and the good agreement (RMSE = 0.724 °C) indicates that our TTOP-derived values are comparable to MAGT at that depth. When MAGT reaches 0 °C, the permafrost layer no longer has any "cold reserve" to resist heat intrusion; the ground temperature profile becomes nearly vertical, signaling that the permafrost is approaching complete thaw. Considering the insulating effects of vegetation and snow cover, which may locally delay thaw, our projections—especially under high-emission scenarios—should be viewed as pessimistic (upper-bound) estimates; the actual degradation may proceed more slowly than simulated due to thermal inertia and buffering feedback.

The QM method used in this study assumes a time invariant bias structure between the historical and future periods, which may not fully hold under non-analogue future climates. More advanced bias-correction techniques, such as Quantile Delta Mapping (QDM), better preserve the climate change signal and will be explored in future work. In Tong et al.'s analysis of future changes under RCP4.5, QM altered the magnitude and spatial pattern of the simulated future change signal to some extent [53]. In contrast, QDM effectively preserved the climate change signal for all extreme indices. Byun and Hamlet [54] introduced a new QM method for inferring future extremes during bias correction, preserving the rank order of simulated future extremes, ensuring bias-corrected values are not exaggerated, retaining the rank structure of the original simulated data, and maintaining the climate change signal in the bias-corrected output. Furthermore, because some of the selected GCMs share model components, a more advanced weighting scheme, such as the Climate model Weighting by Independence and Performance (ClimWIP) approach, is recommended to reduce redundancy and better represent model independence. These improvements will be addressed in subsequent research.

5. Conclusions

This study integrated a Random Forest-based land surface temperature simulation, QM downscaling, and the TTOP model driven by CMIP6 multi-model ensembles to project the long-term evolution of permafrost on the Tibetan Plateau at a 1 km resolution from 1979 to 2100. The results show a continuous warming trend and accelerating permafrost degradation over the past four decades, with more than 20% of the 1979 permafrost area already lost. Future degradation is strongly scenario-dependent: under the low-emission SSP1–2.6 pathway, permafrost loss is limited, while under the high-emission SSP5–8.5 pathway, more than 80% of the current permafrost is projected to disappear by 2100, with the remaining permafrost largely confined to the highest elevations of the Kunlun and Qilian Mountains. Elevation-zone analysis confirms that high-altitude regions act as permafrost refugia, whereas low- and mid-elevation permafrost is highly vulnerable. Sensitivity analyses of soil thermal conductivity indicate that parametric uncertainty leads to a wide range of possible outcomes under high-emission scenarios, but the qualitative conclusion of severe degradation remains robust. The methodological framework demonstrates improved predictive capability over conventional approaches. These findings provide a scientific basis for sustainable engineering construction, infrastructure planning, ecological protection, and climate adaptation in the cold regions of the TP, contributing to the long-term sustainability of the TP under global warming.

Author Contributions: Conceptualization, S.Z.; methodology, J.W. and S.Z.; software, J.W.; validation, J.W. and S.Z.; formal analysis, J.W.; investigation, S.Z.; resources, S.Z.; data curation, J.W.; writing—original draft preparation, J.W.; writing—review and editing, S.Z.; visualization, J.W.; supervision, S.Z.; project administration, S.Z.; funding acquisition, S.Z. All authors have read and agreed to the published version of the manuscript.

Funding: This research was funded by the National Natural Science Foundation of China (42271432) and the Natural Science Foundation of Shanxi Province (202403021211007).

Institutional Review Board Statement: Not applicable.

Informed Consent Statement: Not applicable.

Data Availability Statement: Data will be made available on request.

Acknowledgments: Authors thank the Geospatial Data Cloud site Computer Network Information Center, Chinese Academy of Sciences for providing MODIS land products, and National Tibetan Plateau/Third Pole Environment Data Center for data on glacier, lake, and air temperature on the Tibetan Plateau.

Conflicts of Interest: The authors declare no conflicts of interest.

Abbreviations

The following abbreviations are used in this manuscript:

TTOP	The temperature at the top of permafrost
CMIP6	Coupled model intercomparison project phase 6
MAGT	Mean annual ground temperature
QM	Quantile mapping
RF	Random forest
TP	Tibetan plateau

References

1. Muller, S.W. *Permafrost or Permanently Frozen Ground and Related Engineering Problems*; Strategic Engineering Study, Special Report No. 62; US Engineering Office: Washington, DC, USA, 1943; 136p.
2. Washburn, A.L. *Geocryology*; Edward Arnold: London, UK, 1979; 406p.
3. Zhao, L.; Hu, G.; Liu, G.; Zou, D.; Wang, Y.; Xiao, Y.; Du, E.; Wang, C.; Xing, Z.; Sun, Z.; et al. Investigation, Monitoring, and Simulation of Permafrost on the Qinghai-Tibet Plateau: A Review. *Permafr. Periglac. Process.* **2024**, *35*, 412–422. [CrossRef]
4. Immerzeel, W.W.; van Beek, L.P.H.; Bierkens, M.F.P. Climate Change Will Affect the Asian Water Towers. *Science* **2010**, *328*, 1382–1385. [CrossRef]
5. Immerzeel, W.W.; Lutz, A.F.; Andrade, M.; Bahl, A.; Biemans, H.; Bolch, T.; Hyde, S.; Brumby, S.; Davies, B.J.; Elmore, A.C.; et al. Importance and Vulnerability of the World's Water Towers. *Nature* **2020**, *577*, 364–369. [CrossRef] [PubMed]
6. Zhang, C.; Qin, D.-H.; Zhai, P.-M. Amplification of Warming on the Tibetan Plateau. *Adv. Clim. Change Res.* **2023**, *14*, 493–501. [CrossRef]
7. Biskaborn, B.K.; Smith, S.L.; Noetzli, J.; Matthes, H.; Vieira, G.; Streletskiy, D.A.; Schoeneich, P.; Romanovsky, V.E.; Lewkowicz, A.G.; Abramov, A.; et al. Permafrost Is Warming at a Global Scale. *Nat. Commun.* **2019**, *10*, 264. [CrossRef] [PubMed]
8. Zhang, J.; Chen, J.; Li, C.; Lu, W.; Hao, J.; Niu, P.; Li, K.; Ma, S.; Yuan, R. Landslides along the Engineering Corridors in the Northeastern Margin of the Qinghai-Tibet Plateau of China: Comprehensive Inventory and Mechanism Analysis. *Landslides* **2024**, *21*, 3049–3067. [CrossRef]
9. Miao, Y.; Liu, H.; Song, J.; Dai, T. Research Progress of Transportation Facilities Construction and Their Impact Assessment in the Qinghai Tibet Plateau. *Adv. Earth Sci.* **2020**, *35*, 308–318. (In Chinese) [CrossRef]
10. Zhang, Z.; Wu, Q.; Jiang, G.; Gao, S.; Chen, J.; Liu, Y. Changes in the Permafrost Temperatures from 2003 to 2015 in the Qinghai-Tibet Plateau. *Cold Reg. Sci. Technol.* **2020**, *169*, 102904. [CrossRef]
11. Wu, Q.; Zhang, T.; Liu, Y. Permafrost Temperatures and Thickness on the Qinghai-Tibet Plateau. *Glob. Planet. Change* **2010**, *72*, 32–38. [CrossRef]
12. Zou, D.; Zhao, L.; Sheng, Y.; Chen, J.; Hu, G.; Wu, T.; Wu, J.; Xie, C.; Wu, X.; Pang, Q.; et al. A New Map of Permafrost Distribution on the Tibetan Plateau. *Cryosphere* **2017**, *11*, 2527–2542. [CrossRef]
13. Aalto, J.; Karjalainen, O.; Hjort, J.; Luoto, M. Statistical Forecasting of Current and Future Circum-Arctic Ground Temperatures and Active Layer Thickness. *Geophys. Res. Lett.* **2018**, *45*, 4889–4898. [CrossRef]
14. Marcer, M.; Duvillard, P.-A.; Tomaškovičová, S.; Nielsen, S.R.; Revil, A.; Ingeman-Nielsen, T. Modelling Present and Future Rock Wall Permafrost Distribution in the Sisimiut Mountain Area, West Greenland. *Cryosphere* **2024**, *18*, 1753–1771. [CrossRef]
15. Zhao, S.-P.; Nan, Z.-T.; Huang, Y.-B.; Zhao, L. The Application and Evaluation of Simple Permafrost Distribution Models on the Qinghai–Tibet Plateau. *Permafr. Periglac. Process.* **2017**, *28*, 391–404. [CrossRef]
16. Wang, T.; Yang, D.; Fang, B.; Yang, W.; Qin, Y.; Wang, Y. Data-Driven Mapping of the Spatial Distribution and Potential Changes of Frozen Ground over the Tibetan Plateau. *Sci. Total Environ.* **2019**, *649*, 515–525. [CrossRef]
17. Wang, G.; Niu, S.; Yan, D.; Liang, S.; Su, Y.; Wang, W.; Yin, T.; Sun, X.; Wan, L. Simulation of Active Layer Thickness Based on Multi-Source Remote Sensing Data and Integrated Machine Learning Models: A Case Study of the Qinghai-Tibet Plateau. *Remote Sens.* **2025**, *17*, 2006. [CrossRef]
18. Zhang, X.; Han, L.; Han, L.; Zhu, L. How Well Do Deep Learning-Based Methods for Land Cover Classification and Object Detection Perform on High Resolution Remote Sensing Imagery? *Remote Sens.* **2020**, *12*, 417. [CrossRef]

19. Zhang, Y.; Lackner, R.; Zeiml, M.; Mang, H.A. Strong discontinuity embedded approach with standard SOS formulation: Element formulation, energy-based crack-tracking strategy, and validations. *Comput. Methods Appl. Mech. Engrg.* **2015**, *287*, 335–366. [CrossRef]
20. Zhang, Y.; Huang, J.; Yuan, Y.; Mang, H.A. Cracking elements method with a dissipation-based arc-length approach. *Finite Elem. Anal. Des.* **2021**, *195*, 103573. [CrossRef]
21. Gong, T.; Gao, B.; Ji, Z.; Cao, H.; Zhang, Y. Variation of Active Layer Thickness of Permafrost in the Qinghai-Tibetan Plateau Based on MODIS Temperature Product. *Geogr. Sci.* **2022**, *42*, 1848–1856. [CrossRef]
22. Smith, M.W.; Riseborough, D.W. Climate and the Limits of Permafrost: A Zonal Analysis. *Permafr. Periglac. Process.* **2002**, *13*, 1–15. [CrossRef]
23. Li, X.; Jin, H.; Sun, L.; Wang, H.; Huang, Y.; He, R.; Chang, X.; Yu, S.; Zang, S. TTOP-model-based Maps of Permafrost Distribution in Northeast China for 1961–2020. *Permafr. Periglac. Process.* **2022**, *33*, 425–435. [CrossRef]
24. Li, R.; Zhang, M.; Andreeva, V.; Pei, W.; Zhou, Y.; Misailov, I.; Basharin, N. Impact of Climate Warming on Permafrost Changes in the Qinghai-Tibet Plateau. *Cold Reg. Sci. Technol.* **2023**, *205*, 103692. [CrossRef]
25. Zhao, Y.; Yao, Y.; Jin, H.; Li, X.; Cao, B.; Ran, Y.; Kuang, X.; Zheng, C. TTOP Model Simulation of Long-Term (1981–2100) Permafrost Dynamics of the Tibetan Plateau. *Geoderma* **2025**, *457*, 117–287. [CrossRef]
26. Teutschbein, C.; Seibert, J. Bias Correction of Regional Climate Model Simulations for Hydrological Climate-Change Impact Studies: Review and Evaluation of Different Methods. *J. Hydrol.* **2012**, *456*, 12–29. [CrossRef]
27. Han, Z.; Yao, T.; Gao, X.; Xu, Y. Correction based on quantile mapping for temperature simulated by the RegCM4. *Clim. Change Res.* **2018**, *14*, 331–340. [CrossRef]
28. Ji, F.; Fan, L.-F.; Yuan, S.-S.; Kuang, X.-X.; Zhu, L.-J.; Jin, J.-L.; Yao, Y.-Y.; Zhang, J.-Y.; Zheng, C.-M. Permafrost-Vegetation Controls on Water Availability over the Qinghai-Tibet Plateau. *Adv. Clim. Change Res.* **2025**, *16*, 526–537. [CrossRef]
29. Cheng, G.; Wu, T. Responses of Permafrost to Climate Change and Their Environmental Significance, Qinghai-Tibet Plateau. *J. Geophys. Res. Earth Surf.* **2007**, *112*, F02S03. [CrossRef]
30. Smith, M.W.; Riseborough, D.W. Permafrost Monitoring and Detection of Climate Change. *Permafr. Periglac. Process.* **1996**, *7*, 301–309. [CrossRef]
31. Romanovsky, V.E.; Osterkamp, T.E. Interannual variations of the thermal regime of the active layer and near-surface permafrost in northern Alaska. *Permafr. Periglac. Process.* **1995**, *6*, 313–335. [CrossRef]
32. Cannon, A.J.; Sobie, S.R.; Murdock, T.Q. Bias Correction of GCM Precipitation by Quantile Mapping: How Well Do Methods Preserve Changes in Quantiles and Extremes? *J. Clim.* **2015**, *28*, 6938–6959. [CrossRef]
33. Enayati, M.; Bozorg-Haddad, O.; Bazrafshan, J.; Hejabi, S.; Chu, X. Bias Correction Capabilities of Quantile Mapping Methods for Rainfall and Temperature Variables. *J. Water Clim. Change* **2020**, *12*, 401–419. [CrossRef]
34. Thrasher, B.; Maurer, E.P.; McKellar, C.; Duffy, P.B. Technical Note: Bias Correcting Climate Model Simulated Daily Temperature Extremes with Quantile Mapping. *Hydrol. Earth Syst. Sci.* **2012**, *16*, 3309–3314. [CrossRef]
35. Breiman, L. Random Forests. *Mach. Learn.* **2001**, *45*, 5–32. [CrossRef]
36. Obu, J.; Westermann, S.; Bartsch, A.; Berdnikov, N.; Christiansen, H.H.; Dashtseren, A.; Delaloye, R.; Elberling, B.; Etzelmüller, B.; Kholodov, A.; et al. Northern Hemisphere Permafrost Map Based on TTOP Modelling for 2000–2016 at 1 km^2 Scale. *Earth-Sci. Rev.* **2019**, *193*, 299–316. [CrossRef]
37. Niu, F.; Yin, G. Map of the frozen soil in the Tibetan Plateau. *Natl. Tibet. Plateau/Third Pole Environ. Data Cent.* **2018**. [CrossRef]
38. He, J.; Yang, K.; Tang, W.; Lu, H.; Qin, J.; Chen, Y.; Li, X. The First High-Resolution Meteorological Forcing Dataset for Land Process Studies over China. *Sci. Data* **2020**, *7*, 25. [CrossRef]
39. Yang, K.; He, J.; Tang, W.; Qin, J.; Cheng, C.C.K. On Downward Shortwave and Longwave Radiations over High Altitude Regions: Observation and Modeling in the Tibetan Plateau. *Agric. For. Meteorol.* **2010**, *150*, 38–46. [CrossRef]
40. Eyring, V.; Bony, S.; Meehl, G.A.; Senior, C.A.; Stevens, B.; Stouffer, R.J.; Taylor, K.E. Overview of the Coupled Model Intercomparison Project Phase 6 (CMIP6) Experimental Design and Organization. *Geosci. Model Dev.* **2016**, *9*, 1937–1958. [CrossRef]
41. Cui, T.; Li, C.; Tian, F. Evaluation of temperature and precipitation simulations in CMIP6 models over the Tibetan Plateau. *Earth Space Sci.* **2021**, *8*, e2020EA001620. [CrossRef]
42. Zhang, W.; Liu, L.; Li, X.; Cheng, L.; Cheng, Y.; Li, H. Intensified response of extreme precipitation to rising temperature over the Tibetan Plateau from CMIP6 multi-model ensembles. *J. Hydrol.* **2024**, *639*, 131397. [CrossRef]
43. Kersten, M.S. *Laboratory Research for the Determination of the Thermal Properties of Soils*; University of Minnesota, Engineering Experiment Station: Minneapolis, MN, USA, 1949. Available online: https://hdl.handle.net/11299/124271 (accessed on 28 May 2026).
44. Zhao, L.; Hu, G.; Zou, D.; Wu, T.; Du, E.; Liu, G.; Xiao, Y.; Li, R.; Pang, Q.; Qiao, Y.; et al. A synthesis dataset of permafrost for the Qinghai-Xizang (Tibet) Plateau, China (2002–2018). *Natl. Tibet. Plateau/Third Pole Environ. Data Cent.* **2021**. [CrossRef]
45. Ran, Y.; Li, X.; Cheng, G.; Nan, Z.; Che, J.; Sheng, Y.; Wu, Q.; Jin, H.; Luo, D.; Tang, Z.; et al. Mapping the Permafrost Stability on the Tibetan Plateau for 2005–2015. *Sci. China Earth Sci.* **2021**, *64*, 62–79. [CrossRef]

46. He, R.; Wang, J.; Liu, D. Assessing the Impact of Urban Spatial Form on Land Surface Temperature Using Random Forest—Taking Beijing as a Case Study. *Land* **2025**, *14*, 1639. [CrossRef]
47. Guo, L.; Ran, Y.; Li, X.; Jin, H.; Cheng, G. Sensitivity of Permafrost Degradation to Geological and Climatic Conditions. *Permafr. Periglac. Process.* **2024**, *35*, 450–460. [CrossRef]
48. Liu, Y.; Wu, X.; Wu, T.; Hu, G.; Zou, D.; Qiao, Y.; Wei, X.; Fan, X.; Yan, X. Climate Warming Controls Vegetation Growth with Increasing Importance of Permafrost Degradation in the Northern Hemisphere During 1982–2022. *Remote Sens.* **2025**, *17*, 104. [CrossRef]
49. Yin, G.-A.; Luo, J.; Niu, F.-J.; Liu, M.-H.; Gao, Z.-Y.; Dong, T.-C.; Ni, W.-H. Environmental Factors Controlling Soil Warming and Wetting during 2000–2020 in Permafrost and Non-Permafrost Regions across the Qinghai–Tibet Plateau. *Adv. Clim. Change Res.* **2024**, *15*, 285–296. [CrossRef]
50. Krishna, A.B.; Kaur, P.; Kaur, S.; Kaur, H.; Sandhu, S.S. An Assessment of the Statistical Bias Correction Techniques for CSIRO-Mk 3–6-0 Model Rainfall and Temperature in Punjab, India. *Theor. Appl. Climatol.* **2025**, *156*, 388. [CrossRef]
51. Mahanta, K.K.; Pradhan, I.P.; Dhiman, N.; Singh, A.; Shukla, D.P. Investigating the First Case of Permafrost Degraded Subsidence in Lahaul & Spiti Region of Tethyan Himalayas. *Sci. Rep.* **2025**, *15*, 19262. [CrossRef]
52. Wu, X.; Nan, Z.; Zhao, S.; Zhao, L.; Cheng, G. Spatial modeling of permafrost distribution and properties on the Qinghai-Tibet Plateau. *Permafr. Periglac. Process.* **2018**, *29*, 86–99. [CrossRef]
53. Tong, Y.; Gao, X.; Han, Z.; Xu, Y.; Xu, Y.; Giorgi, F. Bias Correction of Temperature and Precipitation over China for RCM Simulations Using the QM and QDM Methods. *Clim. Dyn.* **2021**, *57*, 1425–1443. [CrossRef]
54. Byun, K.; Hamlet, A.F. An Improved Empirical Quantile Mapping Approach for Bias Correction of Extreme Values in Climate Model Simulations. *Environ. Res. Lett.* **2025**, *20*, 014041. [CrossRef]

Disclaimer/Publisher's Note: The statements, opinions and data contained in all publications are solely those of the individual author(s) and contributor(s) and not of MDPI and/or the editor(s). MDPI and/or the editor(s) disclaim responsibility for any injury to people or property resulting from any ideas, methods, instructions or products referred to in the content.